

# Topological black holes in mimetic gravity

Ahmad Sheykhi<sup>1,2\*</sup> and Saskia Grunau<sup>2†</sup>

<sup>1</sup>*Physics Department and Biruni Observatory, Shiraz University, Shiraz 71454, Iran*

<sup>2</sup>*Institut für Physik, Universität Oldenburg,  
Postfach 2503 D-26111 Oldenburg, Germany*

We construct some new classes of topological black hole solutions in the context of mimetic gravity. We study the uncharged and charged black holes, separately. In the absence of a potential for the mimetic field, our solutions can address the flat rotation curves of spiral galaxies and alleviate the dark matter problem without invoking any kind of particle dark matter. Thus, mimetic gravity can provide a theoretical background for understanding flat galactic rotation curves through modification of the Schwarzschild spacetime. We also investigate the casual structure and physical properties of the solutions. The presence of the mimetic field changes the asymptotic behaviour of the spacetime. We observe that in the absence of a potential, our solutions are not asymptotically flat, while, in the presence of a negative constant potential for the mimetic field, the asymptotic behaviour of the solutions can be anti de-Sitter (AdS). Finally, we explore the motion of massless and massive particles and give a list of the types of orbits. We study the differences of geodesic motion in Einstein gravity and in mimetic gravity. In contrast to Einstein gravity, massive particles always move on bound orbits and cannot escape the black hole in mimetic gravity. Furthermore, we find stable bound orbits for massless particles.

## I. INTRODUCTION

One of the most important challenges of modern cosmology is that about 95% of the total energy content of our Universe is dark and the nature of these dark components is still unknown. It has been shown that the dark side of the Universe consists of two components called dark energy (about 69%) and dark matter (about 26%) of the energy content. The former has anti-gravity property with negative pressure and is responsible for the acceleration of the Universe expansion, and the latter has no electromagnetic interaction but contributes to the gravitational interaction. Indeed, it is now well established that the baryonic matter of galaxies and clusters of galaxies does not provide sufficient gravitation to explain the observed dynamics of the systems and the presence of dark matter is necessary for explanation of such dynamics. Furthermore, according to our

---

\* asheykhi@shirazu.ac.ir

† saskia.grunau@uni-oldenburg.de

present understanding, dark matter has also significant contribution to the anisotropies in the cosmic microwave background, galaxy cluster velocity dispersions, large-scale structure distributions, gravitational lensing investigations, and X-ray measurements from galaxy clusters.

Of course, it is quite possible to deal with the problem in a different perspective. Indeed, one can argue that dark matter might be a manifestation of a theory of gravity beyond General Relativity and does not really consist of particles. In this regard, modified theories of gravity have been proposed to explain gravitational lensing, flat rotation curves of galaxies and dynamics of cluster of galaxies as a geometrical effect. Modified Newtonian Mechanics (MOND) is a known example, which try to explain the flat rotation curves of galaxies, through modifying Newton's law of gravity [1]. However, this theory suffers to embed within a more comprehensive relativistic theory of gravity. Another attempt for probing dark matter through a geometrical effect is the  $f(R)$  theory of gravity, which has been investigated widely in the literature (see e.g. [2–10] and references therein).

A new approach to address the dark matter puzzle, as a geometrical effect was proposed in [11]. This theory, which was first initiated by Chamseddine and Mukhanov [11], called "*mimetic dark matter*" and later became well-known as *mimetic gravity*. One is able to construct mimetic gravity from General Relativity by isolating the conformal degree of freedom of the gravitational field in a covariant way and re-parameterizing the physical metric in terms of an auxiliary metric and a scalar field [11]. In this way, on a flat Friedmann-Robertson-Walker (FRW) Universe, the extra scalar longitudinal degree of freedom of the gravitation field, can be interpreted as the energy density of the mimetic field which scales as  $a^{-3}$ , where  $a$  is the scale factor, thus mimicking the contribution of pressureless dust, without invoking any kind of particle matter [11]. The studies on the mimetic gravity have gained considerable attention in two directions. In the context of cosmology, the dynamical behavior of mimetic gravity with a general potential for the mimetic scalar field has been explored in [12, 13]. It was argued that by adding a non-minimal coupling between matter and the mimetic field, a MOND-like acceleration law in mimetic gravity can be recovered and the flat rotation curves of spiral galaxies are alleviated without needing particle dark matter [14]. It was also pointed out that a modified version of mimetic gravity, can resolve the singularities in contracting Friedmann and Kasner universes and leads to a universe with limiting curvature and regular bounce [15]. Other studies on mimetic gravity in cosmological setups have been carried out in [16–18]. In the context of black hole physics, while Reissner-Nordström black holes in mimetic  $f(R)$  gravity have been explored in [19], static and spherically symmetric solutions in mimetic gravity have been considered in [20, 21]. It was argued that a modified version of this

theory can remove the physical singularity inside the Schwarzschild black hole and results in a geodesically complete spacetime [22]. When a black hole has flat or cylindrical horizon, static and rotating solutions with zero curvature boundary, in mimetic gravity, have been studied in [23]. Black hole spacetimes for both spherically and flat horizon with/without cosmological constant, in mimetic gravity, have also been considered in [24]. The obtained solutions in [23, 24] coincide with the well-known solutions of General Relativity, since they have proposed  $\mathbf{g}_{tt} = -\mathbf{g}^{rr}$ . However, there are more general solutions of the field equations of mimetic gravity. In fact, as it was already pointed out [20, 21], and we shall see shortly, in mimetic gravity, the general solutions can be constructed provided one takes  $\mathbf{g}_{tt} \neq -\mathbf{g}^{rr}$ . This is due to the fact that mimetic field induces an extra degree of freedom to the gravitational field equations which must reflect in the line elements of metric. In this way spherically symmetric black hole solutions in the framework of mimetic gravity were constructed in [20, 21, 25–27].

On the other side, it is well-known that the topology of the event horizon of an asymptotically flat stationary black hole in four dimensions is uniquely determined to be the two-sphere  $S^2$  [28, 29]. Indeed, Hawking’s theorem requires the integrated Ricci scalar curvature with respect to the induced metric on the event horizon to be positive [28]. Of course, when the spacetime is not asymptotically flat, the spherical topology of the black holes horizon is not necessary and one can have stationary black holes with nontrivial topologies. It was argued that for asymptotically AdS spacetime, in the four-dimensional Einstein-Maxwell theory, there exist black hole solutions whose event horizons may have zero or negative constant curvature and their topologies are no longer the two-sphere  $S^2$  (see e.g. [30–35] and references therein).

Despite a lot of efforts in exploring the mimetic gravity, one important question remains to be answered. Is it possible to reproduce the flat galactic rotation curves, in a static spacetime, in mimetic gravity? Our aim in this work is to construct topological black hole solutions in the context of mimetic gravity. For completeness, we study the case of uncharged and charged black holes in the absence and presence of a constant potential for the mimetic field. We find that in order to fully satisfy the field equations, the mimetic potential should be regarded as a negative constant which can admit an asymptotically anti-de Sitter (AdS) spacetime. We also calculate the orbital velocity of a test particle in mimetic spacetime and show that it can serve as an alternative explanation of the flat rotation curves of spiral galaxies. Our work differs from [14] in that we consider the original version of mimetic theory introduced in [11] to explain the flat galactic rotation curves, while the author of [14] reproduces the MOND-like theory within the framework of mimetic gravity, by adding a non-minimal coupling between the mimetic field and the matter hydrodynamic flux.

Our work also differs from [21] where by implementing linear and quadratic corrections to the potential of the mimetic field, they modified the effective Newtonian gravitational potential felt by a test particle. Here, we disclose that in order to explain the flat galactic rotation curves in mimetic gravity, one does not need to add neither a non-minimal coupling term to the action nor taking into account a potential for the mimetic field. We will also analyze our solutions by exploring the orbits of test particles and light, which is a powerful method to study the structure and properties of a spacetime. With the help of geodesics observable quantities like the shadow of a black hole can be calculated and compared to observations. This allows to test different models and theories of gravity. We will derive the equations of motion using the Hamilton-Jacobi approach and study the behaviour of the geodesics with effective potential techniques.

This paper is structured as follows. In the next section, by varying the action of mimetic gravity, we derive the basic field equations. In section III, we obtain topological black hole solutions in mimetic gravity and study the physical properties, asymptotic behaviour and casual structure of the solutions. We also obtain the orbital speed of test particle in mimetic spacetime and show that how it can alleviate the problem of flat rotation curves of spiral galaxies. In section IV, we extend our study to charged topological black holes in the context of mimetic gravity. In section V, we explore the geodesic motion of massless and massive test particles in these spacetimes. We finish with closing remarks in the last section.

## II. BASIC FIELD EQUATIONS

We start with the following action

$$S = \int d^4x \sqrt{-g} [R + \lambda(g^{\mu\nu} \partial_\mu \phi \partial_\nu \phi - \epsilon) - V(\phi) + \mathcal{L}_m], \quad (1)$$

where  $R = R(g_{\mu\nu})$  is the Ricci scalar,  $V(\phi)$  is the potential for the scalar field,  $\lambda$  is the Lagrange multiplier, and  $\mathcal{L}_m = -F_{\mu\nu} F^{\mu\nu}$  is the Lagrangian of the Maxwell field. Here  $F_{\mu\nu} = \partial_\mu A_\nu - \partial_\nu A_\mu$  is the electromagnetic field tensor and  $A_\mu$  is the gauge potential, and  $\epsilon = \pm 1$  depends on the spacelike or timelike nature of  $\partial_\mu \phi$ . Through this paper we take the signature  $(-, +, +, +)$ , thus  $\epsilon = -1$  corresponds to timelike  $\partial_\mu \phi$  and  $\epsilon = 1$  indicates spacelike  $\partial_\mu \phi$ . We further assume  $8\pi G_N = 1$ , unless we mention explicitly. Varying the above action with respect to the metric  $g_{\mu\nu}$  and the scalar field  $\phi$ , leads to the following equations of motion

$$G_{\mu\nu} = \lambda \partial_\mu \phi \partial_\nu \phi - \frac{1}{2} g_{\mu\nu} V(\phi) + T_{\mu\nu} = T_{\mu\nu}^\phi + T_{\mu\nu} \quad (2)$$

$$\nabla^\mu(\lambda\partial_\mu\phi) = -\frac{1}{2}\frac{dV(\phi)}{d\phi}, \quad (3)$$

where the energy momentum tensor of the scalar and electromagnetic field are defined,

$$T_{\mu\nu}^\phi = \lambda\partial_\mu\phi\partial_\nu\phi - \frac{1}{2}g_{\mu\nu}V(\phi), \quad (4)$$

$$T_{\mu\nu} = 2F_{\mu\gamma}F_\nu{}^\gamma - \frac{1}{2}g_{\mu\nu}F_{\alpha\beta}F^{\alpha\beta}, \quad (5)$$

while the equation of motion for the gauge field can be obtained as

$$\partial_\mu(\sqrt{-g}F^{\mu\nu}) = 0. \quad (6)$$

Variation of the action (1) with respect to the Lagrange multiplier  $\lambda$  leads

$$g^{\mu\nu}\partial_\mu\phi\partial_\nu\phi = \epsilon. \quad (7)$$

This implies that the scalar field is always constrained by Eq. (7) and thus is not dynamical by itself, but induces mimetic dark matter in Einstein theory making the longitudinal degree of freedom of the gravitational field dynamical [15]. The mimetic gravity proposed in [11] corresponds to  $\epsilon = -1$  which means that  $\partial_\mu\phi$  should be timelike (their signature differs from ours). We emphasize that introducing  $\phi$  does not add a new dynamical scalar field. This is the main difference between mimetic gravity and standard scalar-tensor theories of gravity such as Brans-Dicke or dilaton gravity where the scalar field adds a new degree of freedom. In contrast, in mimetic gravity, in addition to two transverse degrees of freedom describing gravitons, the gravitational field acquires an extra longitudinal degree of freedom induced by the mimetic field [11]. Thus, mimetic gravity can be viewed as a modification of General Relativity in the longitudinal sector.

Taking the trace of Eq. (2) and using the constraint equation (7), we find

$$\lambda = \epsilon(G - T + 2V), \quad (8)$$

where  $G = G^\mu{}_\mu$  and  $T = T^\mu{}_\mu$  are, respectively, the trace of the Einstein tensor and energy momentum tensor. Inserting  $\lambda$  in the field Eqs. (2) and (3), we arrive at

$$G_{\mu\nu} = \epsilon(G - T + 2V)\partial_\mu\phi\partial_\nu\phi - \frac{1}{2}g_{\mu\nu}V(\phi) + T_{\mu\nu} \quad (9)$$

$$\nabla^\mu[(G - T + 2V)\partial_\mu\phi] = -\frac{\epsilon}{2}\frac{dV(\phi)}{d\phi}. \quad (10)$$

Our aim here is to find the topological static black hole solutions of the above field equations. We assume the line elements of the metric as

$$ds^2 = -g^2(r)f(r)dt^2 + \frac{dr^2}{f(r)} + r^2d\Omega_k^2, \quad (11)$$

where  $f(r)$  and  $g(r)$  are unknown functions of  $r$  which should be determined, and  $d\Omega_k^2$  is the line element of a two-dimensional hypersurface  $\Sigma$  with constant curvature,

$$d\Omega_k^2 = \begin{cases} d\theta^2 + \sin^2\theta d\varphi^2, & \text{for } k = 1, \\ d\theta^2 + d\varphi^2, & \text{for } k = 0, \\ d\theta^2 + \sinh^2\theta d\varphi^2, & \text{for } k = -1. \end{cases} \quad (12)$$

For  $k = 1$ , the topology of the event horizon is the two-sphere  $S^2$ , and the spacetime has the topology  $R^2 \times S^2$ . For  $k = 0$ , the topology of the event horizon is that of a torus and the spacetime has the topology  $R^2 \times T^2$ . For  $k = -1$ , the surface  $\Sigma$  is a 2-dimensional hypersurface  $H^2$  with constant negative curvature. In this case the topology of spacetime is  $R^2 \times H^2$ .

Using the metric (11), the constraint equation (7) yields

$$f(r)\phi'^2 = \epsilon, \rightarrow \phi(r) = \pm \int \frac{dr}{\sqrt{\epsilon f(r)}} + \text{const.}, \quad (13)$$

which again confirms that the scalar field  $\phi$  is not dynamical. For timelike  $\partial_\mu\phi$  ( $\epsilon = -1$ ), the scalar field is imaginary. However, since  $\phi$  is not a dynamical field, it does not make any trouble and we have still a real spacetime. Suppose the gauge potential is in the form  $A_\mu = h(r)\delta_\mu^0$ , and using the metric (11), the only non-vanishing component of Eq. (6) is given by

$$-rE(r)g'(r) + 2E(r)g(r) + rE'(r)g(r) = 0, \quad (14)$$

where  $F_{tr} = E(r) = h'(r)$  is the electric field and the prime denotes the derivative with respect to  $r$ . Solving the above equation for  $E(r)$ , we find

$$E(r) = \frac{q}{r^2}g(r), \quad (15)$$

where  $q$ , which is a constant of integration, is related to the electric charge of the black hole. Inserting metric (11) and the electric field (15) into the field equations (9), regardless the sign of  $\epsilon$ , we obtain the following equations for the components of the Einstein equations,

$$r^3 f' - kr^2 + fr^2 + r^4 V(\phi)/2 + q^2 = 0, \quad (16)$$

$$3r^3 g f' + 2r^3 f g' - kr^2 g + r^2 g f + 3r^4 f' g' + 2r^4 f g'' + r^4 g f'' + 3r^4 g V(\phi)/2 - q^2 g = 0, \quad (17)$$

$$2r^3 (fg)' + 3r^4 f' g' + 2r^4 f g'' + r^4 g f'' + r^4 g V(\phi) - 2q^2 g = 0. \quad (18)$$

In the remaining part of this paper, we are going to solve the above field equations and obtain the unknown functions  $f(r)$  and  $g(r)$ . Clearly, our solutions should also satisfy Eq. (10) for the scalar field. Through this paper, we take two values for the potential of the mimetic field, namely

$V(\phi) = 0$  and  $V(\phi) = -V_0 = -2\Lambda$  with  $\Lambda > 0$ . We also find out that our solutions do not exist for the case of a positive constant potential. Besides, when the mimetic potential is a function of  $r$ , namely for  $V(r) = V[\phi(r)]$ , it is not easy to find an exact analytical solution for the full field equations. Although in [21], the authors considered several type of variable potentials and presented some *approximate* solutions, but their solutions are not the exact solutions of the full field equations and could be only valid for some range of the distance  $r$ . Thus, we leave the solutions of the topological mimetic black holes for a variable potential for future studies.

### III. UNCHARGED BLACK HOLES

In this section, we consider the case where our black hole solutions have no charge by setting  $q = 0$  in the field equations (16)-(17).

#### A. Solutions with $V(\phi) = 0$

At first we investigate the case where  $V(\phi) = 0$ . In this case the field equations reduce to

$$r f' + f - k = 0, \quad (19)$$

$$3 r g f' + 2 r f g' - k g + g f + 3 r^2 f' g' + 2 r^2 f g'' + r^2 g f'' = 0, \quad (20)$$

$$2 (f g)' + 3 r f' g' + 2 r f g'' + r g f'' = 0. \quad (21)$$

The solution to Eq. (19) is given by

$$f(r) = k - \frac{m}{r}. \quad (22)$$

Inserting this solution into Eq. (20), we find the following solution for the metric function

$$g(r) = 1 + b_0 \left[ -2 \left( 1 - \frac{km}{r} \right)^{-1/2} + \ln \left( \frac{r}{r_0} + \frac{r}{r_0} \sqrt{1 - \frac{km}{r} - \frac{km}{2r_0}} \right) \right], \quad \text{for } k = \pm 1, \quad (23)$$

$$g(r) = 1 + b_1 r^{3/2} \quad \text{for } k = 0, \quad (24)$$

where  $b_0$ ,  $b_1$  and  $r_0$  are integration constants. One can easily check that solutions (13), (22) and (23) also satisfy the remaining field equations (10) and (21). The black hole horizon can be obtained from equation  $\mathbf{g}^{rr} = f(r) = 0$ , which has a solution only for the case  $k = +1$ . For  $k = 0, -1$  the solutions do not represent a black hole and we encounter a naked singularity. In order to have a better insight to the nature of the solution, let us calculate the  $(tt)$  component of the metric

function. From the line element (11), we have  $\mathbf{g}_{tt} = -B(r) = -f(r)g^2(r)$ , where

$$B(r) = \left(k - \frac{m}{r}\right) \left\{ 1 + b_0 \left[ -2 \left(1 - \frac{km}{r}\right)^{-1/2} + \ln \left( \frac{r}{r_0} + \frac{r}{r_0} \sqrt{1 - \frac{km}{r} - \frac{km}{2r_0}} \right) \right] \right\}^2, \text{ for } k = \pm 1,$$

$$B(r) = -\frac{m}{r} \left(1 + b_1 r^{3/2}\right)^2 \text{ for } k = 0. \quad (25)$$

Clearly for  $k = 0, -1$  we have always  $\mathbf{g}_{tt} > 0$ , which means the signature of the metric is changed. Again, we confirm that, in mimetic gravity similar to Einstein gravity, we have no topological black holes in the case of zero potential and the horizon topology must be a 2-sphere.

In order to check the curvature singularity of the spacetime, we examine the Ricci and Kretschmann invariants for the obtained solutions. It is easy to show that these invariants diverge at  $r = 0$ , they are finite at  $r \neq 0$  and go to zero for  $r \rightarrow \infty$ . Thus there is a curvature singularity located at  $r = 0$ .

It is also interesting to study the behaviour of the metric function at far distances. Of course, we are aware that in the weak gravitational field regime,  $B(r) \approx 1 + 2\Phi(r)/c^2$ , where  $\Phi(r)$  is the Newtonian gravitational potential and  $c$  is the speed of light. One also knows that the speed of an orbiting test object in this spacetime is given by

$$v^2(r) = r \frac{d\Phi(r)}{dr} = \frac{1}{2} r c^2 \frac{dB(r)}{dr}. \quad (26)$$

In order to have a better insight on the above behaviour of the circular speed, let us expand  $B(r)$  given in (25) for large values of  $r$ , namely at far distance compared to the horizon radius,  $r \gg m$ . It is a matter of calculation to show that ( $k = 1$ )

$$B(r) \approx c_1 - \frac{m}{r} + c_3 \ln r + c_4 (\ln r)^2 + c_5 \frac{m \ln r}{r} + c_6 \frac{m (\ln r)^2}{r} + O\left(\frac{1}{r^2}\right). \quad (27)$$

where  $c_i = c_i(b_0, r_0)$  are constants such that in the absence of a mimetic field ( $b_0 = 0$ ) we have  $c_i = 0$  for  $i \geq 3$ . The constant  $c_1$  can be absorbed in a redefinition of the time coordinate  $t$  and hence can be set equal to one. Note that the higher order terms are all in the form  $1/r^n$  with ( $n \geq 2$ ), and there is no contribution from the logarithmic term in the higher order terms. As we shall see, the logarithmic terms play a crucial role in the behaviour of the orbital speed of a test particle. Without the logarithmic terms, the orbital speed would be a decreasing function of  $r$  and the flat galactic rotation curves are remained upset.

Substituting  $B(r)$  from Eq. (27) into Eq. (26) one can obtain the functional form of the circular speed  $v(r)$  in terms of  $r$  which depends on the parameters  $c_i$  and  $m$ . However, it is more instructive to plot  $v(r)$  for different values of the parameters. The behaviour of the orbital speed



of a test particle in this spacetime, can be applied for understanding the flat rotation curves of spiral galaxies. This can be achieved by assuming that the underlying theory which describe the spacetime around a galaxy is the mimetic gravity. It is well-known that the circular velocity of spiral galaxies at far distances, at the galaxy outskirts, tends to a constant value. Let us note that in the limiting case where  $b_0 = 0$ , our spacetime reduces to the Schwarzschild one, therefore we realize that  $m = 2G_N M/c^2$ . Besides, for  $c_5 = c_6 = 0$ , our solution (27) restores the one proposed in [2], which implies that, in this case we can define  $c_3 = \lambda_0 = 2.8 \times 10^{-12} \sqrt{M/M_\odot}$  (see Eq. (29)). In order to be more realistic, we consider a typical spiral galaxy with mass  $M = 10^{12} M_\odot$ , and thus  $m = 2 \times 10^{12} G_N M_\odot/c^2$ , where  $G_N = 6.674 \times 10^{-11} m^3 kg^{-1} s^{-2}$  is the Newtonian gravitational constant and  $M_\odot \approx 10^{30} kg$  is the mass of the Sun. Substituting  $m$  in (27), with appropriate choice of the other parameters, we can plot the orbital speed in terms of the distance  $r$  from the galaxy center. We summarize our results in Figs. 1 and 2 where  $r$  is given in unit of “kly”. These figures are compatible with astrophysical data [36–38], although we are not going to give the details of data fitting of our model with observations. Indeed, here we present the ideas, and show how mimetic gravity can provide a theoretical basis for explaining the flat rotation curves of spiral galaxies. The detailed data fitting of the parameters space with observations is left for future studies.

From these figures we observe that the orbital speed crucially depends on the parameters  $c_3$  and  $c_4$  but is not sensitive with respect to the parameters  $c_5$  and  $c_6$ . From Fig. 1, we see that even for  $c_5 = c_6 = 0$  we still have a desired flat galactic rotation curve. We observe that the orbital speed increases for small distances and tends to a constant value at large distances, compatible with astrophysical data [36–38]. Besides, at any distance, the orbital speed  $v(r)$  increases with increasing the parameter  $c_4$  which incorporates the effects of mimetic gravity. The reason for this behaviour originates from the fact that with increasing  $c_4$ , the logarithmic term which comes from mimetic field in the solution (27) grows up. In Fig. 2, however, we keep  $c_5$  and  $c_6$  fixed and allow the parameters  $c_3$  and  $c_4$  to vary. Obviously, with increasing either  $c_3$  or  $c_4$ , the orbital speed increases as well. Of course, when  $b_0 = 0$  ( $c_i = 0$ ), namely for the Schwarzschild spacetime, the orbital speed restores  $v(r) = c\sqrt{m/2r} = \sqrt{G_N M/r}$ , which is a decreasing function of  $r$ . Thus, the impact of the mimetic gravity dramatically changes the behaviour of the orbital speed of a test particle in this spacetime.

A question then may arise: what is the origin of such behaviour of the metric function? In other words, why the spacetime metric can naturally explain the flat rotation curves in mimetic gravity? In order to address this question, let us recall the original work [11] where the idea of *mimetic dark matter* was initiated. In [11], the authors argued that, on the flat FRW Universe

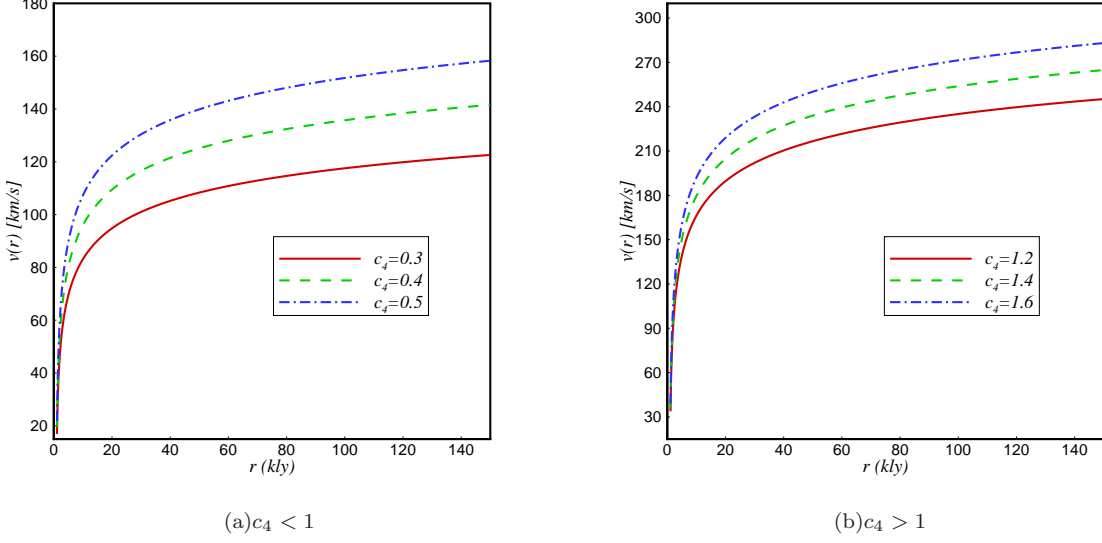


FIG. 1: The circular speed of an orbiting test particle around a typical spiral galaxy with mass  $M = 10^{12} M_{\odot}$  in the mimetic spacetime in terms of distance  $r$ . Here, we have taken  $c_5 = c_6 = 0$  and kept fixed  $c_3 = 2.8 \times 10^{-12} \sqrt{M/M_{\odot}} = 2.8 \times 10^{-6}$  [2].

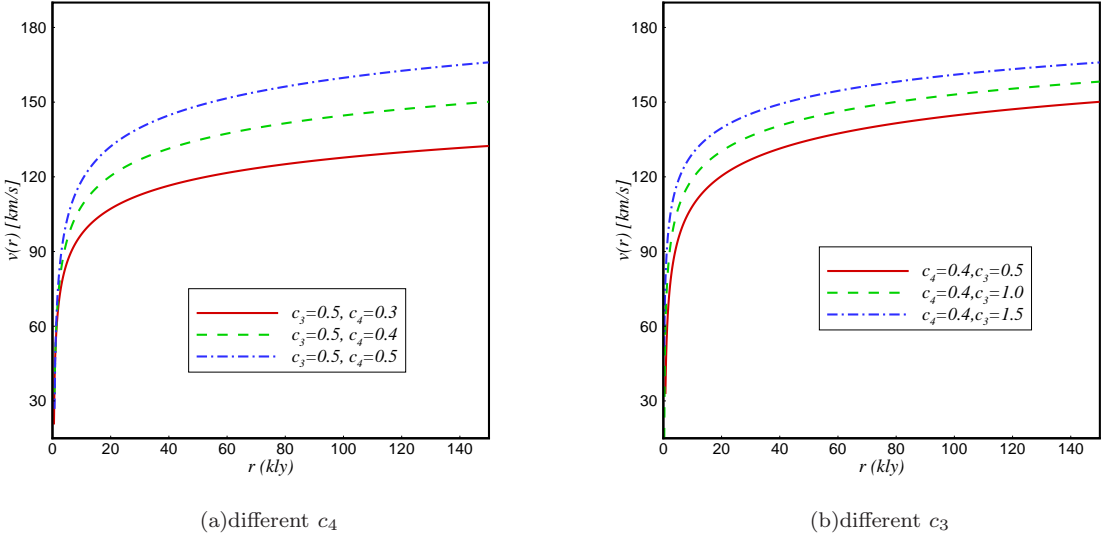


FIG. 2: The circular speed of an orbiting test particle around a typical spiral galaxy with mass  $M = 10^{12} M_{\odot}$  in mimetic spacetime in terms of distance  $r$ . Here, we have taken  $c_5 = c_6 = 2$ .

where the mimetic field is a function of time  $\phi = t$ , the energy density of the mimetic field can be written in the form  $\rho_{mim} = G - T = C(x^i)/a^3$  where  $a$  is the scale factor of the Universe and, thus mimicking the contribution of pressureless dust. The constant  $C(x^i)$  determines the value of the mimetic dark matter. Even, in the absence of matter where  $T = 0$ , this mimetic energy density is equal to  $\rho_{mim} = -R$ , which, in general, has a non-vanishing value. This implies that, in mimetic

gravity, dark matter appears naturally as a purely geometrical effect. This mimetic energy density comes from the extra longitudinal degree of freedom of the gravitational field equation induced by the mimetic field. It is worth noticing that, for consistency, in this picture, one should define the four-velocity of this mimetic dust as  $u^\mu = g^{\mu\nu}\partial_\nu\phi$  which satisfies the normalization condition  $u^\mu u_\mu = \epsilon$ . This means the mimetic field plays the role of the velocity potential. Clearly, the normalization condition for the four-velocity is equivalent to the condition (7) for the mimetic field  $\phi$ . Now we back to the above question. In the context of static spacetime where  $\phi = \phi(r)$ , the field equations admit a solution which can explain the flat galactic rotation curves, but how? Indeed the responsible term for such behaviour is the second term in the metric function (23), namely  $g(r) - 1$ . This term in solution (23) contributes from the mimetic term  $(G - T + 2V)\partial_\mu\phi\partial_\nu\phi$  in the gravitational field Eq. (9), which is indeed the energy-momentum tensor of the mimetic field. Note that in our case,  $V = 0 = T$  and this term is reduced to  $-R\partial_\mu\phi\partial_\nu\phi$ . Without this mimetic term, the field equations admit a unique solution  $g(r) = 1$  and necessary implies  $b_0 = 0$ , which is just the solution of General Relativity.

In order to clarify how the second term in  $g(r)$  reflects the effect of mimetic field, let us note that the functional form of  $g(r)$  in (23), before integrating, is given by

$$g(r) = 1 + b_0 \int \frac{\sqrt{r} dr}{(r - m)^{3/2}} = 1 + b_0 \int \frac{dr}{r[f(r)]^{3/2}} = 1 + b_0 \int r^{-1}[\epsilon\phi'(r)]^3 dr. \quad (28)$$

Obviously, in the absence of mimetic field ( $\phi = 0$ ), the second term vanishes and our solution reduces to that of General Relativity. In conclusion, the origin of the responsible term, which is capable to reproduce the flat galactic rotation curves in a static spacetime, is the one which mimics *dark matter* in the cosmological setup [11]. This is the reason why the velocity of a test particle in mimetic gravity, in a static spacetime, can be naturally explained and the inferred flat galactic rotation curves are reproduced without invoking particle dark matter. More precisely, the proposed model of mimetic theory of gravity in [11] is defined in such a way that naturally mimics dark matter as a geometrical effect. Therefore, it is not strange that we could reproduce the flat galactic rotation curves in the background of static spacetime in mimetic gravity, without any modification in the action [14] or taking into account a variable potential [21].

Our work may also provide a theoretical origin for the proposed modification of the Schwarzschild spacetime in Ref. [2] for the explanation of the flat galactic rotation curves. Let us recall that, in order to explain the flat rotation curves of spiral galaxies, the author of [2] proposed that the flat rotation curves of spiral galaxies can be explained by logarithmic gravitational potentials. He assumed the (00) component of the metric around a galaxy, at far distance, in addition

to the Schwarzschild term, should have a logarithmic term,

$$B(r) = 1 - \frac{r_s}{r} + \lambda_0 \ln r. \quad (29)$$

where  $r_s = 2G_N M/c^2$  is the Schwarzschild radius of the galaxy, and  $\lambda_0 \approx 2.8 \times 10^{-12} \sqrt{M/M_\odot}$  [2]. In order to justify the appearance of the logarithmic term in the metric function around a galaxy, the author [2] modified the underlying theory of gravity by adding a new energy momentum tensor to Einstein's field equations. He proposed that a spiral galaxy has a dark perfect fluid companion which provides such modification in the metric. Here, we observe that the mimetic gravity can serve a logarithmic term in the metric function without needing to add a dark companion to the galaxy matter. Indeed, as argued in [11], the extra longitudinal degree of freedom of the gravitation field, in mimetic gravity, is responsible for the appearance of such a logarithmic term in the metric function which could have naturally appeared at far distances. Thus, in our work the dark matter can be understood as a geometrical impact. Finally, we emphasize that in Eq. (27), we present the next correction terms to the Schwarzschild metric which comes from the longitudinal degree of freedom of the gravitational field in mimetic gravity.

### B. Solutions with $V(\phi) = -2\Lambda$

Next, we consider the case in the presence of a constant potential for the scalar field. Indeed, the consistent solutions, which fully satisfy the field equations, only exist for the case  $\Lambda > 0$ . In this case the field Eqs. (16)-(18) with  $q = 0$ , admit the following solutions

$$f(r) = k - \frac{m}{r} + \frac{\Lambda r^2}{3}, \quad \text{for } k = 0, \pm 1, \quad (30)$$

$$g(r) = 1 + b_2 \frac{r^{3/2}}{\sqrt{\Lambda r^3 - 3m}} \quad \text{for } k = 0, \quad (31)$$

$$g(r) = 1 + c_0 \int \frac{\sqrt{r} dr}{(\Lambda r^3 - 3m + 3kr)^{3/2}}, \quad \text{for } k = \pm 1. \quad (32)$$

The horizon can be obtained from  $g^{rr} = f(r) = 0$ . For  $k = 0$ , black hole has a single horizon located at  $r_h = (3m/\Lambda)^{1/3}$ , and from (31) we observe that  $g(r) \rightarrow \infty$  at  $r = r_h$ . However, this is just a coordinate singularity and all curvature invariants are finite at  $r = r_h$ . For  $k = \pm 1$ , however, the horizon is the real positive root of  $\Lambda r^3 - 3m + 3kr = 0$ . In these cases, we have again one horizon located at  $r_+$  where its radius depends on the parameters  $m$  and  $\Lambda$ . We have also a coordinate singularity at  $r_+$ , as one can see from solution (32).

Again, it is a matter of calculations to show that these solutions together with (13) fully satisfy the field equation for the scalar field given in (10). Since the integral in Eq. (32), cannot be done

analytically, we expand the integrand for large values of  $r$ . We find

$$g(r) \approx 1 + \frac{c_0}{\Lambda^{5/2} r^5} \left\{ \frac{9k}{10} - \frac{\Lambda r^2}{3} - \frac{3m}{4r} + O\left(\frac{1}{r^2}\right) \right\}, \quad \text{for } k = \pm 1. \quad (33)$$

Similarly, the function  $B(r) = f(r)g^2(r) = -\mathbf{g}_{tt}$  at large distance is obtained

$$\begin{aligned} B(r) &= \frac{\left(\sqrt{\Lambda r^3 - 3m} + b_2 r^{3/2}\right)^2}{3r} \\ &\approx \frac{r^2}{3} \left(\Lambda + b_2^2 + 2b_2\sqrt{\Lambda}\right) - \frac{m}{r} \left(1 + \frac{b_2}{\sqrt{\Lambda}}\right) + O\left(\frac{1}{r^4}\right) \quad \text{for } k = 0, \end{aligned} \quad (34)$$

$$B(r) \approx k - \frac{m}{r} + \frac{\Lambda r^2}{3} - \frac{2c_0}{9\sqrt{\Lambda}} \frac{1}{r} + O\left(\frac{1}{r^3}\right) \quad \text{for } k = \pm 1. \quad (35)$$

We observe that for a flat horizon ( $k = 0$ ),  $B(r)$  has a minimum value  $B(r)|_{\min} = b_2^2 r_h^2 / 3 = b_2^2 (3m/\Lambda)^{2/3} / 3$  at the horizon. Besides, from solution (34) we see that, for  $k = 0$ , the asymptotic behaviour is *approximately* AdS, unless in the absence of the mimetic field ( $b_2 = 0$ ), where the asymptotic behaviour of the spacetime is AdS. On the other hand, from solutions (30) and (35) we see that for  $k = \pm 1$ , as  $r \rightarrow \infty$ , we have  $\mathbf{g}^{rr} = -\mathbf{g}_{tt} = k + \Lambda r^2 / 3$ , which confirms that the spacetime is asymptotically AdS. A close look on solution (35) shows that an extra term  $c_0/r$  is added to the metric, compared to the topological black hole in Einstein gravity. This leading order term incorporates the effects of the mimetic field on the spacetime geometry far from the horizon. Calculating the curvature scalars of this spacetime indicates that

$$\lim_{r \rightarrow 0^+} R = \infty, \quad (36)$$

$$\lim_{r \rightarrow 0^+} R_{\mu\nu\rho\sigma} R^{\mu\nu\rho\sigma} = \infty, \quad (37)$$

while, for the asymptotic region where  $r \rightarrow \infty$ , the invariants of the spacetime are obtained as

$$\lim_{r \rightarrow \infty} R = -4\Lambda, \quad (38)$$

$$\lim_{r \rightarrow \infty} R_{\mu\nu\rho\sigma} R^{\mu\nu\rho\sigma} = \frac{8}{3}\Lambda^2. \quad (39)$$

The behaviour of the metric functions for topological black holes in mimetic gravity are shown in Figs. 3 and 4. From Fig. 3 we see that the black hole has one horizon and the radius of this horizon increases with increasing the mass parameter  $m$ . On the other hand, Fig. (4a) indicates that  $g(r) \rightarrow -\infty$  for small  $r$  goes to unity for large values of  $r$ . This is an expected result, since at large distance, we expect the effects of the mimetic field to disappear. Fig. (4b) also shows that a black hole has one infinite redshift surface which is the root of  $B(r) = 0$  and its radius decreases with increasing  $\Lambda$ .

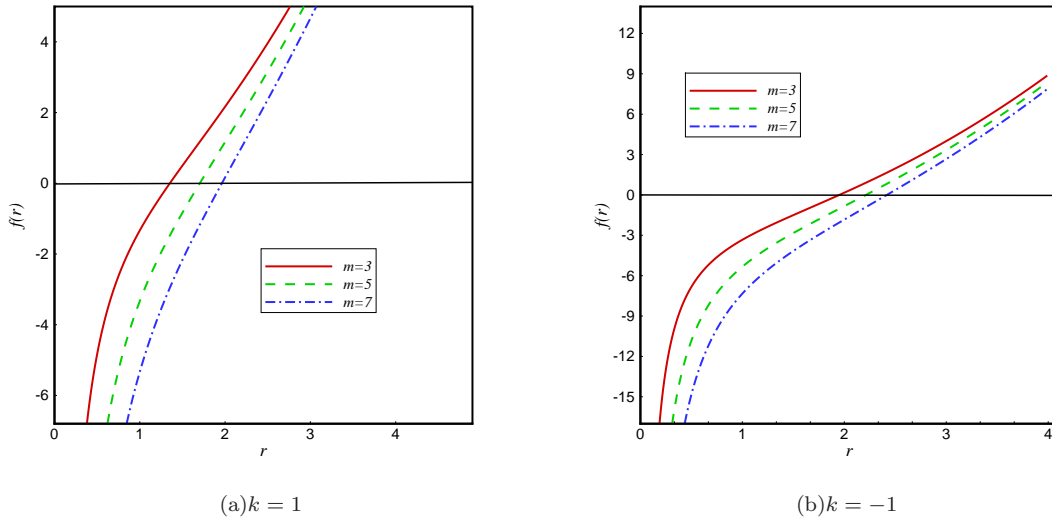


FIG. 3: The behavior of  $f(r)$  for a topological black hole in the presence of a constant potential with  $\Lambda = 2$ .

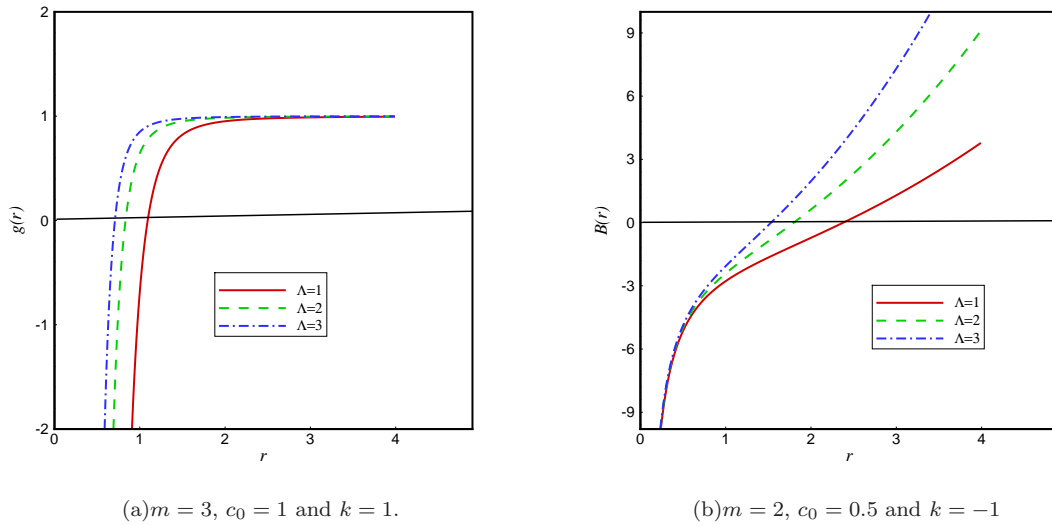


FIG. 4: The asymptotic behavior of the metric functions  $g(r)$  (left) and  $B(r) = f(r)g^2(r)$  (right) for a topological black hole with different  $\Lambda$ .

#### IV. CHARGED BLACK HOLES

In this section we would like to consider the possible solutions for charged topological black holes in the context of mimetic gravity.

### A. Solution with $V(\phi) = 0$

To have a better insight on the nature of the solutions we first consider the case with zero potential. In this case Eqs. (16)-(18) have the following solutions

$$f(r) = k - \frac{m}{r} + \frac{q^2}{r^2}, \quad \text{for } k = 0, \pm 1 \quad (40)$$

$$g(r) = 1 + B_0 \frac{m^2 r^2 + 4q^2 r m - 8q^4}{\sqrt{mr - q^2}}, \quad \text{for } k = 0,$$

$$g(r) = 1 + A_0 \left\{ \ln \left( \frac{r}{r_0} + \frac{\sqrt{r^2 - k(mr - q^2)}}{r_0} - \frac{km}{2r_0} \right) - \frac{2(m^2 r - 2kq^2 r - mq^2)}{(m^2 - 4kq^2)\sqrt{r^2 - k(mr - q^2)}} \right\}, \quad \text{for } k = \pm 1, \quad (41)$$

where  $B_0$ ,  $A_0$  and  $r_0$  are constants of integration. In this case we have a black hole solution for  $k = 1$ . For  $k = 0, -1$ , however, we have no black hole solution and one may encounter with a naked singularity covered by a cosmological horizon. Indeed, in these cases the metric function changes its sign,  $f(r) < 0$ , for  $r > r_c$  as one can see in Fig. (5b). For  $k = 1$ , however, we have two horizons located at,

$$r_{\pm} = \frac{1}{2} \left( m \pm \sqrt{m^2 - 4q^2} \right). \quad (42)$$

Thus, for spherical topology, we have a black hole with an inner and an outer horizon for  $m > 2q$ , an extremal black hole for  $m = 2q$ , and a naked singularity for  $m < 2q$  (see Fig. 5a).

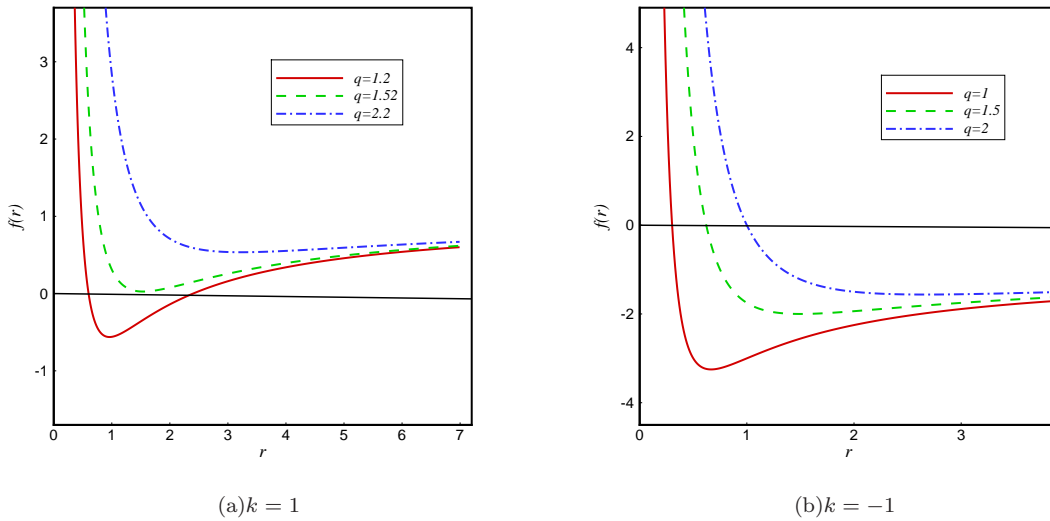


FIG. 5: The behavior of  $f(r)$  for a charged topological black hole with  $m = 3$  and different  $q$ .

Next, we study the behaviour of the metric function  $B(r) = f(r)g^2(r)$  for large values of  $r$ . It

is a matter of calculation to show that for  $k = \pm 1$ , at far distance,

$$B(r) \approx = A_1 + A_2 \ln\left(\frac{r}{r_0}\right) + A_3 \frac{\ln r}{r} + \frac{A_4}{r} + \dots, \quad (43)$$

while for  $k = 0$ ,  $B(r) \approx B_1 r^2 + B_2 r + \dots$  which diverges as  $r \rightarrow \infty$ . This might be due to the presence of the mimetic field  $\phi$ . Here  $A_i$  and  $B_i$  are constants which are functions of  $m$ ,  $r_0$ ,  $q$ ,  $B_0$  and  $A_0$ . In conclusion, in the absence of a potential, we have charged black hole solutions only for spherical horizon topology ( $k = 1$ ), and in other cases ( $k = 0, -1$ ) we encounter a naked singularity with a cosmological horizon. In all cases the spacetime is asymptotically neither flat nor AdS due to the presence of the mimetic field.

### B. Solutions with $V(\phi) = -2\Lambda$

Finally, we consider charged topological black holes in the presence of a potential for the mimetic field. In this case Eqs. (16)-(18) admit the following solutions

$$f(r) = k - \frac{m}{r} + \frac{q^2}{r^2} + \frac{\Lambda r^2}{3}, \quad \text{for } k = 0, \pm 1 \quad (44)$$

$$g(r) = 1 + C_0 \int \frac{r^2 dr}{(3kr^2 + \Lambda r^4 - 3mr + 3q^2)^{3/2}}, \quad \text{for } k = 0, \pm 1 \quad (45)$$

where  $C_0$  is a constant of integration. The integral in the expression (45) cannot be done analytically, so we expand the integrand for large  $r$  limit. It is a matter of calculations to show that

$$g(r) \approx 1 + \frac{C_0}{\Lambda^{5/2} r^5} \left\{ \frac{9k}{10} - \frac{\Lambda r^2}{3} - \frac{3m}{4r} + \frac{9q^2}{14r^2} - \frac{135|k|}{56\Lambda r^2} + \dots \right\}, \quad (46)$$

which yields

$$B(r) = f(r)g^2(r) \approx k - \frac{m}{r} - \frac{2C_0}{9\sqrt{\Lambda}r} + \frac{q^2}{r^2} + \frac{\Lambda r^2}{3} + \dots \quad (47)$$

Clearly, in the asymptotic region where  $r \rightarrow \infty$ , we have  $g(r) \approx 1$  and  $\mathbf{g}^{rr} = -\mathbf{g}_{tt} = k + \Lambda r^2/3$ , which confirms that the asymptotic behaviour of the obtained solutions is AdS. Comparing the above solution with the solution of Einstein gravity in the presence of a cosmological constant, here, we have an additional term  $-\frac{2C_0}{9\sqrt{\Lambda}r}$  which incorporates the effect of the mimetic field through the constant  $C_0$ . If we redefine the mass parameter such as  $m' = m + 2C_0/(9\sqrt{\Lambda})$ , then the above solution reduces to

$$B(r) \approx k - \frac{m'}{r} + \frac{q^2}{r^2} + \frac{\Lambda r^2}{3} + \dots \quad (48)$$



Let us have a look at the electric field of the spacetime. From Eq. (15), we have

$$E(r) = \frac{q}{r^2}g(r) \approx \frac{q}{r^2} \left\{ 1 + \frac{C_0}{\Lambda^{5/2}r^5} \left[ \frac{9k}{10} - \frac{\Lambda r^2}{3} - \frac{3m}{4r} + \frac{9q^2}{14r^2} - \frac{135|k|}{56\Lambda r^2} + \dots \right] \right\} \quad (49)$$

Thus, far from the black hole, the electric field behaves as  $E(r) \sim q/r^2$ , since in this regime we have  $g(r) \approx 1$ . Again the Ricci and Kretschmann invariants diverge at  $r = 0$ , they are finite for  $r \neq 0$  and go to  $-4\Lambda$  and  $4\Lambda^2/3$ , respectively, for  $r \rightarrow \infty$ . Thus, we confirm that the essential singularity is at  $r = 0$ .

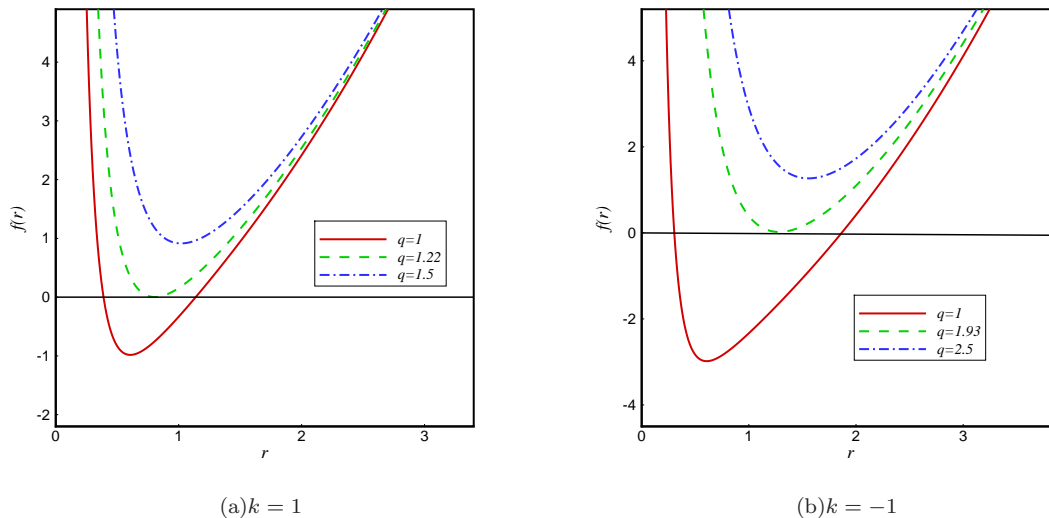


FIG. 6: The behavior of  $f(r)$  for a charged topological black hole in the presence of a constant potential with  $\Lambda = 2$ ,  $m = 3$ .

The behavior of the metric functions and the electric field for charged topological black holes in mimetic gravity are plotted in Figs. 6 and 7. From Fig. 6, we observe that our solutions can represent, depending on the metric parameters, black holes with an inner and an outer horizon, an extremal black hole, or naked singularity. Similar behaviour is also seen for the cases with  $k = 0$ . In Fig. (7a), we also plotted the behaviour of the electric field, where it is observed that, for small  $r$  the electric field diverges, while it goes to zero for large values of  $r$ , as one expects. Finally, from Fig. (7b), we see that  $g(r)$  diverges for small values of  $r$  and goes to unity for large values of  $r$ .

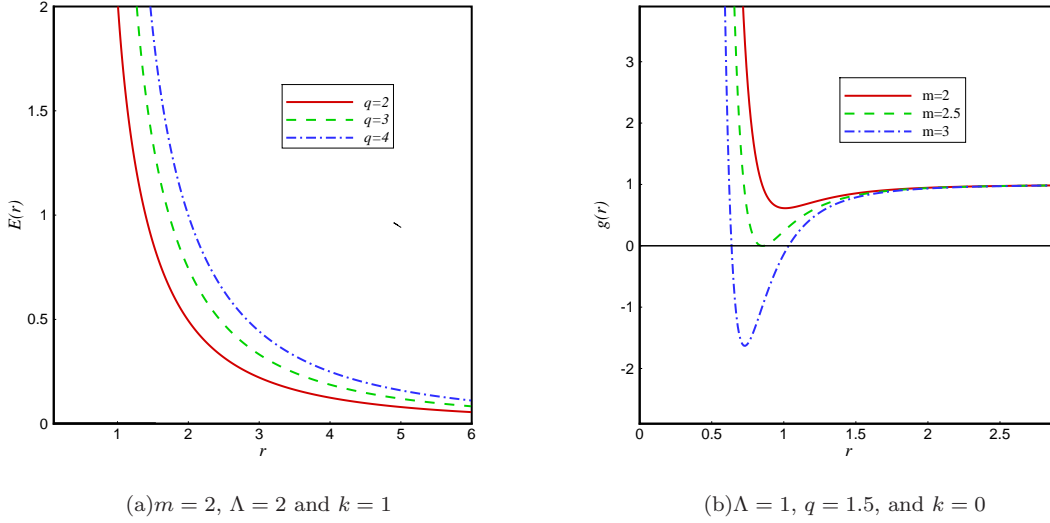


FIG. 7: The behavior of the electric field  $E(r)$  (left) and  $g(r)$  (right) for a charged topological black hole in the presence of a constant potential with  $C_0 = 1$ .

## V. GEODESICS MOTION AROUND MIMETIC BLACK HOLES

In this section we study the geodesic motion of massless and massive particles in the spacetimes of mimetic black holes. For symmetry reasons we can choose  $\theta$  to be constant. In the case  $k = 1$  we will choose the equatorial plane  $\theta = \frac{\pi}{2}$  and in the case  $k = -1$  we will choose  $\theta = \ln(1 + \sqrt{2})$  so that  $\sinh(\theta) = 1$ . Then in all three cases  $k = 1, 0, -1$  we will have  $g_{\varphi\varphi} = r^2$ .

We derive the equations of motion using the Hamilton-Jacobi formalism. To solve the Hamilton-Jacobi equation

$$\frac{1}{2}g^{\mu\nu}\frac{\partial S}{\partial x^\mu}\frac{\partial S}{\partial x^\nu} + \frac{\partial S}{\partial \tau} = 0, \quad (50)$$

we use the following ansatz for the action

$$S = \frac{1}{2}\delta\tau - Et + L\varphi + S_r(r), \quad (51)$$

where  $\tau$  is an affine parameter along the geodesics. For massive particles we have  $\delta = 1$  and for massless particles  $\delta = 0$ .  $E$  is the energy and  $L$  is the angular momentum of the test particle.

With the above ansatz and the metric (11) the Hamilton-Jacobi equation becomes

$$\delta - \frac{E^2}{f(r)g(r)^2} + \frac{L^2}{r^2} + f(r)\left(\frac{\partial S_r}{\partial r}\right)^2 = 0, \quad (52)$$

and therefore

$$\left(\frac{\partial S_r}{\partial r}\right) = \sqrt{-\frac{\delta}{f(r)} - \frac{L^2}{f(r)r^2} + \frac{E^2}{f(r)^2g(r)^2}}. \quad (53)$$

We can derive the equations of motion by varying the action with respect to the constants of motion

$$\left(\frac{dr}{d\varphi}\right)^2 = \frac{r^4 E^2}{L^2 g(r)^2} - r^2 f(r) \left(\frac{\delta r^2}{L^2} - 1\right), \quad (54)$$

$$\left(\frac{dr}{dt}\right)^2 = f(r)^2 g(r)^2 - \frac{f(r)^3 g(r)^4}{E^2} \left(\delta + \frac{L^2}{r^2}\right). \quad (55)$$

From equation (54) we can define an effective potential  $V_{\text{eff}}$  by

$$\left(\frac{dr}{d\phi}\right)^2 = \frac{r^4}{L^2 g(r)^2} (E^2 - V_{\text{eff}}) \quad (56)$$

which yields

$$V_{\text{eff}} = \left(\delta + \frac{L^2}{r^2}\right) f(r) g(r)^2. \quad (57)$$

### A. Uncharged black holes with $V(\phi) = 0$

First we will consider uncharged black holes with  $V(\phi) = 0$ . We insert the metric functions (22) and (23) the case  $k = 1$ , which describes a spherical black hole in mimetic gravity. The  $r(\phi)$  equation of motion and the effective potential are

$$\begin{aligned} \left(\frac{dr}{d\varphi}\right)^2 &= \frac{E^2 r^4}{L^2} \left\{ 1 + b_0 \left[ -2 \left(1 - \frac{m}{r}\right)^{-1/2} + \ln \left( \frac{r}{r_0} \left( +\sqrt{1 - \frac{m}{r}} \right) - \frac{m}{2r_0} \right) \right] \right\}^{-2} \\ &\quad - r^2 \left(1 - \frac{m}{r}\right) \left(\frac{\delta r^2}{L^2} - 1\right), \end{aligned} \quad (58)$$

$$V_{\text{eff}} = \left(\delta + \frac{L^2}{r^2}\right) \left(1 - \frac{m}{r}\right) \left\{ 1 + b_0 \left[ -2 \left(1 - \frac{m}{r}\right)^{-1/2} + \ln \left( \frac{r}{r_0} \left( +\sqrt{1 - \frac{m}{r}} \right) - \frac{m}{2r_0} \right) \right] \right\}^2. \quad (59)$$

Apparently equation (58) can only be solved with numerical methods. However, we can analyse the effective potential (59) to study the behaviour of the geodesics. Figure 8 shows some plots of the effective potential (59) for different values of  $b_0$ . We see that for every  $b_0$  all potentials meet at the same point  $(r_p, V_{\text{eff}}(r_p))$ , which can be calculated by

$$r_0 \exp \left( \frac{2}{\sqrt{1 - \frac{m}{r_p}}} \right) = r_p \sqrt{1 - \frac{m}{r_p}} - \frac{m}{2} + r_p. \quad (60)$$

Furthermore, if  $g(r_c) = 0$ , then  $V_{\text{eff}}(r_c) = \frac{dV_{\text{eff}}}{dr}(r_c) = 0$  and there is a stable circular orbit with zero energy. The position  $r_c$  of the circular orbit can be calculated by

$$r_0 \exp \left( \frac{2b_0 - \sqrt{1 - \frac{m}{r_p}}}{b_0 \sqrt{1 - \frac{m}{r_p}}} \right) = r_p \sqrt{1 - \frac{m}{r_p}} - \frac{m}{2} + r_p. \quad (61)$$

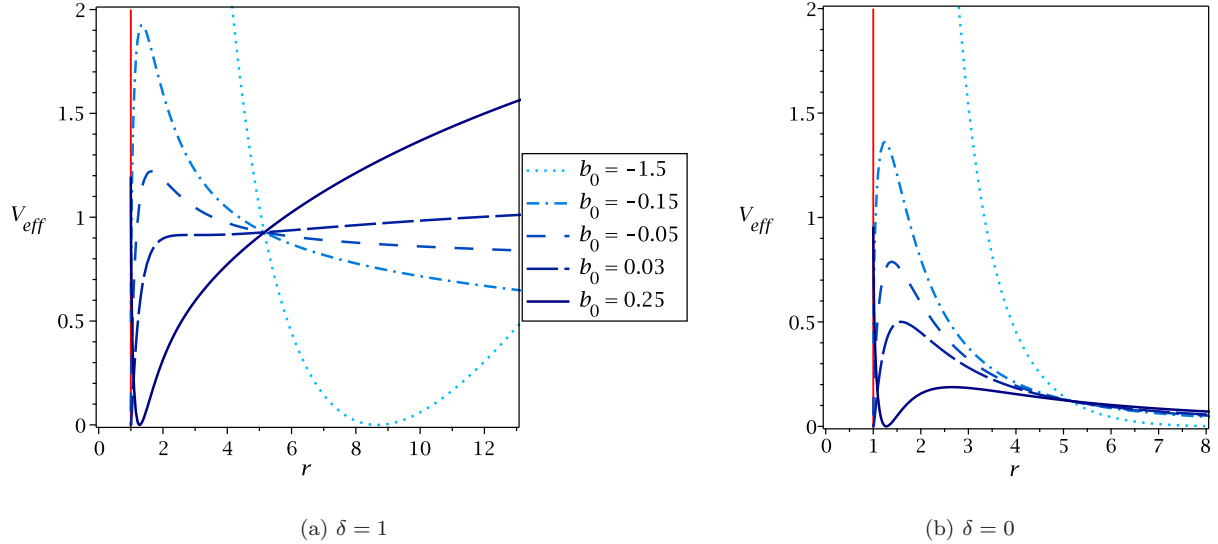


FIG. 8: Effective potential (59) for test particles moving around an uncharged black hole with  $V(\phi) = 0$  and  $k = 1$ ,  $m = 1$ ,  $L = 2$ ,  $r_0 = 1$ . The blue curves represent the effective potential for different values of  $b_0$  and the red vertical line indicates the position of the event horizon. Figure (a) is the effective potential for massive particles and figure (b) is the effective potential for light.

Due to the logarithmic term, the effective potential diverges for  $r \rightarrow \infty$  in the case  $\delta = 1$ . This means that all geodesics for massive particles are bound orbits, as long as  $b_0 \neq 0$ . For  $\delta = 0$  the effective potential approaches  $V_{eff} = 0$  for  $r \rightarrow \infty$ , so that light can escape the black hole.

The turning points of the orbits are the zeros of  $\left(\frac{dr}{d\varphi}\right)^2$ . Geodesic motion is possible for  $\left(\frac{dr}{d\varphi}\right)^2 \geq 0$ , which means  $E^2 \geq V_{eff}$ . We find the following orbit configurations for massive particles:

1. A single turning point  $r_1 > r_h$  exists and  $\left(\frac{dr}{d\varphi}\right)^2 \geq 0$  for  $r_1 \geq r \geq 0$ . The corresponding orbit is a terminating bound orbit, which ends in the singularity at  $r = 0$ .
2. Two turning points  $r_2 \geq r_1 > r_h$  exist and  $\left(\frac{dr}{d\varphi}\right)^2 \geq 0$  for  $r_2 \geq r \geq r_1$ . The corresponding orbit is a bound orbit. This configuration does not exist in the Schwarzschild spacetime.
3. Three turning points  $r_3 > r_2 > r_1 > r_h$  exist and  $\left(\frac{dr}{d\varphi}\right)^2 \geq 0$  for  $r_3 \geq r \geq r_2$  and  $r_1 \geq r \geq 0$ . There is a bound orbit with  $r_3 \geq r \geq r_2$  and a terminating bound orbit with  $r_1 \geq r \geq 0$ , which ends in the singularity.

In the case of massless particles the following orbits occur:

1. There is no turning point and  $\left(\frac{dr}{d\varphi}\right)^2 \geq 0$  for  $r \geq 0$ . The light rays coming from infinity fall into the singularity (terminating escape orbit).

2. Two turning points  $r_2 \geq r_1 > r_h$  exist and  $\left(\frac{dr}{d\varphi}\right)^2 \geq 0$  for  $r_1 \geq r$  and  $r \geq r_2$ . A terminating bound orbit and an escape orbit exist.
3. Three turning points  $r_3 > r_2 > r_1 > r_h$  exist and  $\left(\frac{dr}{d\varphi}\right)^2 \geq 0$  for  $r_2 \geq r \geq r_1$  and  $r \geq r_3$ . There is a bound orbit and an escape orbit. This configuration does not exist in the Schwarzschild spacetime.

If the parameter  $|b_0|$  is sufficiently small, the geodesics close to the black hole in mimetic gravity behave similar to those in the Schwarzschild spacetime. However for large  $r$  the logarithmic term dominates, so that in contrast to General Relativity massive particles cannot escape the mimetic black hole. As the parameter  $|b_0|$  grows, the effective potential close to the black hole is no longer similar to Schwarzschild and a minimum at  $E = 0$  appears in the effective potential. Then there are stable circular orbits with zero energy. Moreover, massless particles can move on a stable bound orbit, which is not possible in the Schwarzschild spacetime.

Looking at the sky an observer will see a dark region, the so called shadow, around a black hole. The shadow is a projection of the photon sphere [39], which marks the boundary between light rays escaping the black hole and light rays falling into the black hole. For small  $|b_0|$  there is an unstable circular orbit for photons, which corresponds to the radius of the photon sphere. Here the shadow is very similar to the Schwarzschild spacetime. If we increase  $|b_0|$ , the size of the shadow will change.

For negative  $b_0$  there is still an unstable circular orbit for photons which will be closer to the black hole in comparison to the Schwarzschild case.

For positive  $b_0$ , the situation is more complex. At first, for small  $b_0$  we have an unstable circular orbit for photons, which will be further away from the black hole than in the Schwarzschild case. For increasing  $b_0$  there is a stable circular orbit for photons, but additionally there is an unstable circular orbit for larger  $r$  (see figure 8 of the effective potential). This unstable photon orbit is the photon sphere, which is at a larger distance than in the Schwarzschild case.

Now if we increase  $b_0$  further, we have to take into account, that the effective potential at the event horizon is not zero, as in the Schwarzschild case. At some point the energy value of the effective potential at the horizon will be larger than the energy at the unstable circular photon orbit. This means that light rays can get arbitrarily close to the black hole and still being reflected at the potential barrier (of course at a certain energy they will fall beyond the horizon). In this case the photon sphere has the same size as the horizon.

### B. Charged black holes with $V(\phi) = -2\Lambda$

Here we consider charged spherical black holes with  $V(\phi) = -2\Lambda$ . In this case there are two horizons  $r_+$  and  $r_-$ . We insert the metric functions (44) and (46) in the case  $k = 1$  into the equation of motion (54) and the effective potential (57)

$$\left(\frac{dr}{d\varphi}\right)^2 = \frac{E^2 r^4}{L^2} \left[ 1 + \frac{C_0}{\Lambda^{5/2} r^5} \left( \frac{9}{10} - \frac{\Lambda r^2}{3} - \frac{3m}{4r} + \frac{9q^2}{14r^2} - \frac{135}{56\Lambda r^2} \right) \right]^{-2} - r^2 \left( 1 - \frac{m}{r} + \frac{q^2}{r^2} + \frac{\Lambda r^2}{3} \right) \left( \frac{\delta r^2}{L^2} - 1 \right), \quad (62)$$

$$V_{\text{eff}} = \left( \delta + \frac{L^2}{r^2} \right) \left( 1 - \frac{m}{r} + \frac{q^2}{r^2} + \frac{\Lambda r^2}{3} \right) \left[ 1 + \frac{C_0}{\Lambda^{5/2} r^5} \left( \frac{9}{10} - \frac{\Lambda r^2}{3} - \frac{3m}{4r} + \frac{9q^2}{14r^2} - \frac{135}{56\Lambda r^2} \right) \right]^2. \quad (63)$$

Note that we used the expanded version of the function  $g(r)$  in the large  $r$  limit. For  $r \rightarrow \infty$  the effective potential diverges for massive particles and approaches  $V_{\text{eff}} = \frac{\Lambda L^2}{3}$  for massless particles. At  $r = 0$  there is a potential barrier due to the charge. Figure 9 shows the effective potential for massive particles and light moving around a charged black hole with  $V(\phi) = \Lambda$ .

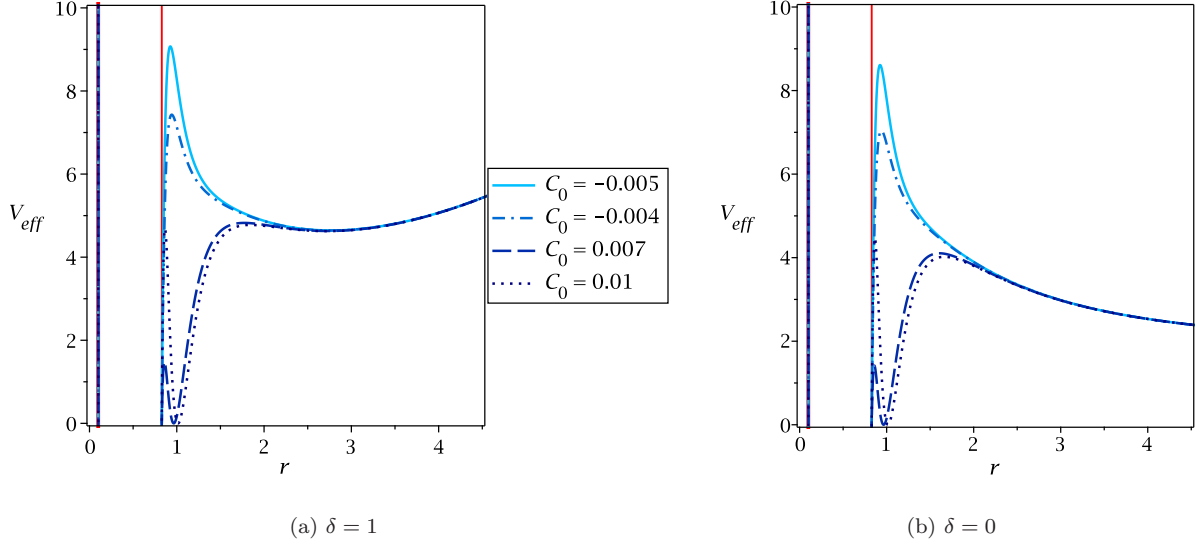


FIG. 9: Effective potential (59) for test particles moving around a charged black hole with  $V(\phi) = \Lambda$  and  $k = 1$ ,  $m = 1$ ,  $L = 4$ ,  $q = 0.3$ ,  $\Lambda = \frac{1}{3}$ . The blue curves represent the effective potential for different values of  $b_0$  and the red vertical lines indicate the position of the horizons. Figure (a) is the effective potential for massive particles and figure (b) is the effective potential for massless particles.

For massive particles we find the following orbit configurations:

1. There are two turning points  $r_1 < r_-$ ,  $r_2 > r_+$  and  $\left(\frac{dr}{d\varphi}\right)^2 \geq 0$  for  $r_1 \leq r \leq r_2$ . The

corresponding orbit is a many-world bound orbit which emerges into another universe each time both horizons are crossed twice.

2. There are four turning points  $r_1 < r_-, r_+ < r_2 < r_3 < r_4$  and  $\left(\frac{dr}{d\varphi}\right)^2 \geq 0$  for  $r_1 \leq r \leq r_2$  and  $r_3 \leq r \leq r_4$ . A many-world bound orbit and a normal bound orbit exist.
3. There are six turning points  $r_1 < r_-, r_+ < r_2 < r_3 < r_4 < r_5 < r_6$  and  $\left(\frac{dr}{d\varphi}\right)^2 \geq 0$  for  $r_1 \leq r \leq r_2$  and  $r_3 \leq r \leq r_4$  and  $r_5 \leq r \leq r_6$ . A many-world bound orbit and two normal bound orbits exist. This configuration does not exist in the Reissner-Nordström AdS spacetime.

For massless particles we find the following orbit configurations:

1. There is a single turning point  $r_1 < r_-$  and  $\left(\frac{dr}{d\varphi}\right)^2 \geq 0$  for  $r \geq r_1$ . The corresponding orbit is a two-world escape orbit which emerges into another universe after crossing both horizons twice.
2. There are three turning points  $r_1 < r_-, r_+ < r_2 < r_3$  and  $\left(\frac{dr}{d\varphi}\right)^2 \geq 0$  for  $r_1 \leq r \leq r_2$  and  $r \geq r_3$ . A many-world bound orbit and an escape bound orbit exist.
3. There are five turning points  $r_1 < r_-, r_+ < r_2 < r_3 < r_4 < r_5$  and  $\left(\frac{dr}{d\varphi}\right)^2 \geq 0$  for  $r_1 \leq r \leq r_2$  and  $r_3 \leq r \leq r_4$  and  $r \geq r_5$ . A many-world bound orbit, a normal bound orbit and an escape orbit exist. This configuration does not exist in the Reissner-Nordström AdS spacetime.

If the parameter  $|C_0|$  is sufficiently small, the geodesics around the black hole in mimetic gravity behave similar to those in the Reissner-Nordström AdS spacetime. As the parameter  $|C_0|$  grows, the effective potential is no longer similar to Reissner-Nordström AdS and a minimum at  $E = 0$  appears in the effective potential. Then there are stable circular orbits with zero energy. Moreover, massless particles can move on a stable bound orbit, which is not possible in the Reissner-Nordström AdS spacetime. Note that the behaviour of the effective potential close to the black hole varies a lot with  $C_0$ , while at large  $r$  the parameter  $C_0$  does not have much influence. For a description of the effects of the size of the photon sphere see previous section.

## VI. CLOSING REMARKS

In [27], Deruelle and Rua showed that, in general, Einstein field equations of General Relativity are invariant under disformations, however, relaxing this invariance can yield the field equations of

mimetic gravity which bring rich physics. In this theory, in contrast to scalar tensor theories, the mimetic field  $\phi$  is not dynamical by itself and is always restricted by Eq. (7). Instead, it induces an extra longitudinal degree of freedom to the gravitation field, in addition to two transverse degrees of freedom describing gravitons. This extra degree of freedom, on the cosmological background, admits an energy density, with geometrical origin, which scales like pressureless matter and thus mimics dark matter [11]. If mimetic energy density resembles dark matter, is it possible to explain the flat galactic rotation curves in this gravity? To answer this question, in this paper, we have studied static black holes in the context of mimetic gravity. For completeness, we considered black hole with various horizon topology including spherical with positive constant curvature, cylindrical with zero curvature and hyperbola with negative constant curvature. In order to reflect the impact of the mimetic field into the spacetime metric, we should require  $\mathbf{g}_{tt} \neq -\mathbf{g}_{rr}^{-1}$ , which means that we allow an extra degree of freedom in the metric line elements.

We have discussed several cases including whether there is or not a constant potential in the background and whether there is or not charge on the black holes. We have explored the casual structure and some physical properties of the solutions. In the absence of potential, these solutions are not asymptotically flat which is due to the presence of the mimetic field  $\phi$ . When a constant potential (cosmological constant) is taken into account, it dramatically affects the behaviour of the spacetime and leads to asymptotically AdS and *approximately* AdS for, respectively, charged and uncharged solutions. Interestingly enough, we have noted that when the horizon is spherical, and in the absence of potential, the spacetime describing by our solution can explain the flat rotation curves of spiral galaxy without invoking particle dark matter. In this viewpoint, the dark matter is indeed a geometrical effect which originate from the extra degree of freedom of gravitational field, induced into the spacetime metric, by the mimetic field. We have discussed the origin of such behaviour of the metric in ample details. In order to quantify our results, we applied our metric to a typical spiral galaxy by assuming that the underlying theory describing the spacetime is mimetic gravity. We have plotted the orbital speed of a test particle, at far distance, at galaxies outskirts, around a typical galaxy with mass  $M = 10^{12} M_{\odot}$ , in terms of the distance which are in good agreement with observational data [37, 38].

We have also analyzed the geodesics motion of massive and massless particles around spherically symmetric black holes in mimetic gravity. We have focused on two cases: the uncharged case with zero potential and the charged case with constant potential,  $V(\phi) = -2\Lambda$ . We have found that if the parameters  $|b_0|$  or  $|C_0|$  are sufficiently small, then the geodesics close to the black hole behave similar to geodesics in Einstein gravity. However, in the uncharged case at large distances the effective



potential differs from Einstein gravity. Here the logarithmic term dominates so that massive particles cannot escape the black hole and will always move on bound orbits. If the parameters  $|b_0|$  or  $|C_0|$  grow, then the motion is no longer similar to geodesics in the Schwarzschild or Reissner-Nordström (AdS) spacetime. We observed that, in mimetic gravity, new orbit configurations appear and there is a minimum with  $E = 0$  in the effective potential, so that stable circular orbits with  $E = 0$  exist. Furthermore, in the spacetime of a mimetic black hole we found stable bound orbits for massless particles, which do not exist in Einstein gravity (in four dimensions). Additionally we found that the size of the photon sphere is smaller than in the Schwarzschild or Reissner-Nordström case for negative  $|b_0|$  or  $|C_0|$  and larger for positive  $|b_0|$  or  $|C_0|$ . However, if  $|b_0|$  or  $|C_0|$  get “too large” that suddenly the photon sphere shrinks to the size of the event horizon.

The explanation of the flat galactic rotation curves, in the background of static spacetime, further supports the viability of mimetic theory of gravity. It confirms that this theory may serve an alternative explanation for the presence of dark matter in the Universe, as pointed out in [11]. Indeed, this investigation is of great importance because, at least, at theoretical level, is an indication that the geometrical origin of dark matter can be understood naturally within a more comprehensive relativistic theory of gravity. Given the wide ranges of the observational data available, in the future, we expect to further constrain our model parameter space and check the viability of mimetic gravity.

### Acknowledgments

We thank Jutta Kunz for useful discussions and valuable comments. AS thanks Shiraz University and also the Institute of Physics of the University of Oldenburg, for hospitality. S.G. gratefully acknowledges support by the DFG (Deutsche Forschungsgemeinschaft/ German Research Foundation) within the Research Training Group 1620 “Models of Gravity.”

- 
- [1] M. Milgrom, *Astrop. J* **270**, 365 (1983).
  - [2] Yousef Sobouti, [arXiv:0810.2198].
  - [3] Yousef Sobouti, *Dark Matter in Astrophys. and Particle Phys.* (2009) 356.
  - [4] T. P. Sotiriou and V. Faraoni, *Rev. Mod. Phys.* **82** (2010) 451 [arXiv:0805.1726].
  - [5] C. G. Boehmer, T. Harko, F. S. N. Lobo, *Astropart. Phys.* **29** (2008) 386, [arXiv:0709.0046]
  - [6] F. Shojai, A. Shojai, *Gen. Relat. Gravit.* **46**, 4, (2014) 1704, [arXiv:1404.0299].
  - [7] J.-h. He, A.J. Hawken, B. Li, L. Guzzo, *Phys. Rev. Lett.* **115**, 071306 (2015), [arXiv:1501.00846].

- [8] R. Zaregonbadi, M. Farhoudi, N. Riazi, Phys. Rev. D **94**, 084052 (2016), [arXiv:1608.00469].
- [9] S. D. Odintsov, V. K. Oikonomou, Phys. Rev. D **99**, 104070 (2019) [arXiv:1905.03496].
- [10] S. D. Odintsov, V. K. Oikonomou, Phys. Rev. D **99**, 064049 (2019) [arXiv:arXiv:1901.05363].
- [11] A. H. Chamseddine and V. Mukhanov, JHEP **1311** (2013) 135.
- [12] A. H. Chamseddine, V. Mukhanov and A. Vikman, JCAP **1406** (2014) 017.
- [13] J. Dutta, et. al., JCAP **1802** (2018) 041.
- [14] S. Vagnozzi, Class. Quant. Grav. **34** (2017) 185006, [arXiv:1708.00603].
- [15] A. H. Chamseddine and V. Mukhanov, JCAP **03**, (2017) 009, [arXiv:1612.05860].
- [16] A.H. Chamseddine, V. Mukhanov, T. B. Russ, Eur. Phys. J. C **79** (2019) 558, [arXiv:1905.01343].
- [17] N. Sadeghnezhad, K. Nozari, Phys. Lett. B **769** (2017) 134, [arXiv:1703.06269];  
M. A. Gorji, S. Mukohyama, H. Firouzjahi, JCAP **05** (2019) 019, [arXiv:1903.04845];  
M. A. Gorji, S. Mukohyama, H. Firouzjahi, S. A. Hosseini, JCAP **08** (2018) 047, [arXiv:1807.06335];  
M. B. Lopez, C.-Y. Chen and P. Chen, **11** (2017) 053, [arXiv:1709.09192];  
M. A. Gorji, S. A. Hosseini, H. Firouzjahi, JCAP **01** (2018) 020, [arXiv:1709.09988]
- [18] L. Sebastiani, S. Vagnozzi and R. Myrzakulov, Adv. High Energy Phys. (2017) 3156915.
- [19] V.K. Oikonomou, Universe **2** (2016) 10 [arXiv:1511.09117]
- [20] R. Myrzakulov, L. Sebastiani, Gen. Rel. Grav. **47**, (2015) 89. [arXiv:1503.04293].
- [21] R. Myrzakulov, et. al., Class. Quant. Grav. **33** (2016) 125005 [arXiv:1510.02284].
- [22] A. H. Chamseddine, V. Mukhanov, Eur. Phys. J. C **77** (2017) 183.
- [23] G.G.L. Nashed, W. E Hanafy and K. Bamba, JCAP **01** (2019) 058, [arXiv:1809.02289]
- [24] G.G.L. Nashed, Symmetry **10**, (2018) 559.
- [25] C.Y. Chen, M. Bouhmadi-López, P. Chen, Eur. Phys. J. C **78** (2018) 59, [arXiv:1710.10638].
- [26] G. G. L. Nashed, Int. J. Geom Met. Mod. Phys. Vol.**15**, No. 09, 1850154 (2018).
- [27] N. Deruelle and J. Rua, JCAP **09**, (2014) 002, [arXiv:1407.0825].
- [28] S. W. Hawking and G. F. Ellis. *The large scale structure of spacetime*. Cambridge University Press, Cambridge, England, (1973).
- [29] S. W. Hawking. Commun. Math. Phys. **25**, 152 (1972).
- [30] J. P. S. Lemos, Phys. Lett. B **353**, 46 (1995).
- [31] R. G. Cai and Y. Z. Zhang, Phys. Rev. D **54**, 4891 (1996).
- [32] D. R. Brill, J. Louko, and P. Peldán, Phys. Rev. D **56**, 3600 (1997).
- [33] R. G. Cai and K. S. Soh, Phys. Rev. D **59**, 044013 (1999).
- [34] R. G. Cai, J.Y. Ji, and K. S. Soh, Phys. Rev. D **57**, 6547 (1998).
- [35] S. Hajkhalili, A. Sheykhi, Phys. Rev. D **99**, 024028 (2019);  
A. Sheykhi, Phys. Lett. B **662** (2008) 7.
- [36] N. P. Vogt, et.al., The Astronomical J., **127** (2004) 3273.
- [37] P. D. Mannheim, J. O'Brien, Phys. Rev. D **85** (2010) 124020, [arXiv:1011.3495].
- [38] J. G. O'Brien and P. D. Mannheim, Mon. Not. Roy. Astron. Soc. **421** (2012) 1273 [arXiv:1107.5229].

- [39] C. M. Claudel, K. S. Virbhadra and G. F. R. Ellis, *J. Math. Phys.* **42**, 818 (2001)